CFD investigation of the radiative heat transfer effects on the adoption of an electrical heated catalyst to increase the abatement efficiency

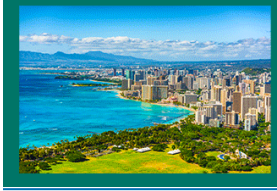

CFD investigation of the radiative heat transfer effects on the adoption of an electrical heated catalyst to increase the abatement efficiency

Loris Barillari, Augusto Della Torre, Gianluca Montenegro, Angelo Onorati

Politecnico di Milano, Department of Energy, Internal Combustion Engines Group, Italy

E-mail: loris.barillari@polimi.it

Abstract. The thermal transient of the after-treatment system (ATS) during the cold start and the typical urban drive low load engine operations is a crucial point for the conversion efficiency. In this context, the adoption of electrical heating is regarded as an effective solution to promote the catalytic activity and the pollutants abatement. This paper focuses on the evaluation of the radiative heat transfer affecting the operation of an electrical heated catalyst employed to increase the abatement efficiency of a standard catalyst. The modeling methodology relies on a CFD framework based on a Conjugate Heat Transfer (CHT) approach in OpenFOAM, so that a detailed characterization of the thermal transient of the different components of the exhaust line can be achieved. The electrical heating device under investigation is based on a metallic support and it is heated by the Joule effect. The distribution of the heat and its subsequent interaction with the gas flow significantly influence the catalyst operations. In this context, the CFD modeling framework has been further developed so that it is possible to accurately evaluate the radiative heat transfer in correspondence of the porous regions. The description of such features is mandatory for an accurate prediction of the maximum electrical heating device temperatures, resulting in a reliable estimation of the gas flow temperature and its subsequent interaction with the catalyst. The simulation methodology has been applied at first excluding the radiative heat transfer. Then, the developed radiation modeling is applied, so that its influence on the ATS performance can be fully evaluated.

1. Introduction

As a response to the environmental pollution, stricter and stricter emission legislations are pushing the automotive sector development. The definition of the future Euro 7 regulation is expected to introduce further restrictions on the admissible pollutants emissions. While different powertrain solutions are proposed, as the outcome of the energy transition and the global diversification of the energy sources, the state-of-the-art internal combustion engines still represent a valuable technology in the automotive sector. The after treatment systems (ATS) of the internal combustion engines play a fundamental role in reducing the tailpipe emissions of the powertrain. With regards to gasoline and Diesel engines, a catalyst is commonly one of the ATS components, as a three way catalyst (TWC) or a Diesel oxidizer catalyst (DOC) respectively. The effectiveness of the pollutants conversion is strictly related to the their brick temperature, that is required to be over 500 K to ensure a sufficient catalytic activity [1]. During the cold start of the engine, the time required to achieve such condition is significant and the cumulative

emissions of the early operations of the engine typically exceed by an order of magnitude the emissions registered after the light-off event [2]. In this context, different solutions are proposed in order to warm up the catalyst. The most common strategies rely on the modifications of the in-cylinder operations to exploit the higher exhaust gas energy [3, 4]. Other approaches are based on specific catalyst heat-up technologies, characterized by the possibility of activating such solution in advance with respect to the engine start [5]. The utilization of burner systems or external combustors is one of those technical solutions, even though still confined at the research stage due to technical challenges [6, 7]. In this context, another heat-up strategy is based on the application of electrical heated catalyst [8, 9, 10].
This paper reports the adoption of a metallic electrical heated catalyst (EHC), focusing on the importance of the radiative heat transfer occuring at the analyzed component. In particular, the device under investigation is meant to be located upstream the conventional catalyst and it is subjected to different pre-heating phases before the engine cold start. The heating strategy results in the progressive increase of the temperature of the device, with a peculiar temperature distribution related to its specific arrangement. In particular, the presence of local hot spots could limit the average temperature of the electrical heater, leading to lower gas temperatures and higher catalyst light-off times. The radiative heat transfer contribution is fundamental for the evolution of the temperature distribution, especially at high temperature. In order to evaluate and appreciate the importance of the radiative heat transfer, a CFD investigation is carried out on a simplified exhaust system line, excluding the conventional after-treatment components. Through a dedicated implementation, it is possible to accurately evaluate the exchanged radiative heat power in correspondence of the porous region. The obtained results are compared to the available experimental measurements of the analogous test bench. For each of the different operating conditions, in terms of electrical power of the EHC, the CFD simulations are carried out neglecting the radiation contributions. Then, the methodology including the radiative heat transfer is employed, providing a clear source of understanding of the radiation relevance for the EHC application.

2. Methodology

The simulation methodology applied in this research relies on a Conjugate Heat Transfer (CHT) multi-region modeling approach, implemented on the basis of the open-source CFD code OpenFOAM. It consists of a further development of an established set of libraries dedicated to the complex analysis of ATS, exploiting overlapping domains and proper coupling models to describe the interaction between the engine gases and the different after-treatment components, namely the porous substrates and the particulate filters [11, 12]. In particular, the geometrical details of the components channels are not represented within the simulation framework: the catalytic substrates or filters are modelled by means of a porous media approach. The general schematization of an ATS component, according to the appointed methodology, is presented in Figure 1(a). It is possible to appreciate the presence of a substrate region, overlapped to the fluid domain, and the external metallic walls of the line. Figure 1(b) presents a similar schematization for an ATS line equipped with an EHC. From the simulation methodology point of view, both the EHC and the substrate domains are modelled by means of the porous media approach.
The interaction between the fluid domain and the standard solid domains, such as the exhaust system metallic walls or insulation layers, is handled through the typical conjugate heat transfer approach implemented within OpenFOAM. As the main outcome of the presented work, the coupling methodology for the porous ATS components is extended in order to effectively include the radiative heat transfer in correspondence of such domains.

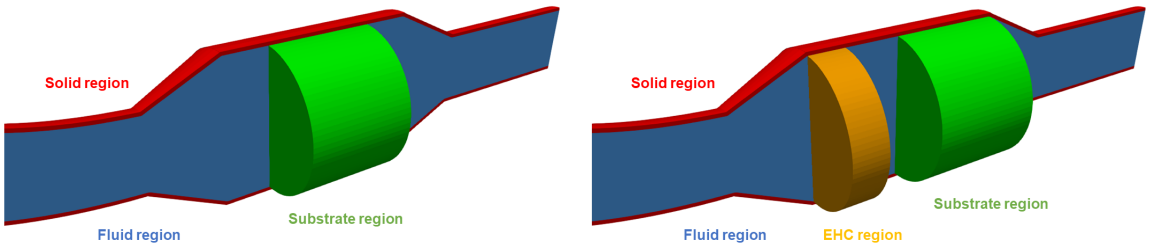

(a) *Simple ATS configuration* **(b)** *Simple ATS configuration with EHC*

Figure 1: Implemented after-treatment system CFD modeling

2.1. Radiation modeling

A comprehensive thermal description of the system can be achieved through the CFD code. The simulation framework allows to tackle all the different heat transfer phenomena, including the radiative heat transfer, according to different modeling approaches. Electromagnetic radiation processes are associated to energy fluxes and, in a conjugate heat transfer analysis, play a fundamental role in the evolution of the thermal transient of the simulated domains. The governing equation for the radiation processes is the radiative transfer equation (RTE), that describes the variation of the spectral thermal radiation intensity in a certain position $\vec{r}$ for a given direction $\vec{s}$. Its complete formulation results in a first order integro-differential equation that depends on three spatial coordinates, two local direction coordinates, time and wavelength [13, 14]. Time dependence is often neglected, assuming local thermodynamic equilibrium (LTE). The resulting equation (1) for i_λ, that is the spectral intensity, as a function of the wavelength λ, the considered direction $\vec{s}$ and solid angle ω, is:

$$\frac{di_\lambda}{d\vec{s}} = a_\lambda i_{\lambda b} - (a_\lambda + \sigma_{s\lambda}) i_\lambda + \frac{\sigma_{s\lambda}}{4\pi} \int_{\omega_i=0}^{4\pi} i_\lambda(\vec{s}, \omega_i) \Phi(\lambda, \omega, \omega_i) d\omega_i \tag{1}$$

where a_λ is the absorption coefficient, $\sigma_{s\lambda}$ the scattering coefficient, Φ the phase function of scattering and $i_{\lambda b}$ the spectral density of the radiation of the medium. The associated complexity is significant; several models have been proposed to provide simplified pratical modeling approaches [13, 15, 16]. OpenFOAM provides different radiation models as well, so that the computational framework can be adapted to the case under investigation according to different assumptions.

As a preliminar development of the simulation methodology, the authors selected the P1 radiation model. It constitutes the simplest case of the P-N approach, that relies on the expansion of the radiation spectral intensity in a series of orthogonal harmonics [13]. Then, the series can be truncated after a finite number of terms N. In case of isotropic scattering, the RTE results in a second order partial differential equation (2) for G, the spectral incident radiation at the position $\vec{r}$, defined as in equation (3).

$$\vec{\nabla} \cdot (\Gamma_\lambda \vec{\nabla} G_\lambda) - a_\lambda G_\lambda + a_\lambda 4\pi i_{\lambda b} = 0 \tag{2}$$

where $\Gamma_\lambda = 1/3K_\lambda$ and K_λ is the spectral extinction coefficient, defined as $a_\lambda + \sigma_{s\lambda}$.

$$G_\lambda(\vec{r}) = \int_{\omega_i=0}^{4\pi} i_\lambda(\vec{r}, \vec{s}) d\omega_i \tag{3}$$

If gray media with constant absorption and extinction coefficients are considered, the RTE is further simplified in a non-linear modified Helmholtz equation (4):

$$\frac{\partial^2 G}{\partial x_j \partial x_j} - 3aKG + 3aK \cdot 4\sigma T^4 = 0 \tag{4}$$

where σ is the Stefan-Boltzmann constant. For diffusive gray surfaces, Marshak boundary condition is employed, evaluating the net radiative heat flux q_w with respect to the walls radiative properties and thermodynamic conditions (5):

$$q_w = -\Gamma \frac{\partial G}{\partial n}\Big|_w = \frac{\epsilon_w}{2(2-\epsilon_w)} \cdot (4\sigma T_w^4 - G_w) \tag{5}$$

where ϵ_w is the wall emissivity. The applicability of the model is related to optical thick media, for which radiation travels a short distance before being absorbed or scattered, with isotropic scattering. If the underling assumptions are not realistic, the model is expected to overestimate the resulting radiation heat fluxes from localized heat sources.

2.2. Radiative heat transfer coupling methodology

The previously referenced CHT simulation methodology is extended to account for the radiative emission from the substrates included in the ATS. As described in the introductory part of Section 2, the ATS substrates are represented according to the porous media approach, through computational domains overlapped to the fluid region. Given the applied simulation methodology, the physical interaction between the overlapping regions is described by means of source terms. Accordingly, the novel radiative heat transfer coupling methodology is obtained through the addition of a proper radiative source term at the interface between the component and the fluid flow. In this way, the contribution associated to the porous domains emissivity can be added to the fluid incident radiation equation; the ATS component radiative emission can propagate within the fluid domain and consistently contribute to the radiative heat transfer. The radiation source term in correspondence of the fluid - porous region interfaces is computed as follow:

$$S_g = C_f A \cdot 4\epsilon e_b \tag{6}$$

where S_g represents the source term, A the porous region boundary area, ϵ the component surface emissivity and e_b its black body emission, equal to σT^4. C_f is a corrective factor, used to increase the area of the considered porous domain boundary. As a matter of fact, the fraction of radiative energy leaving the ATS component is supposed to be associated to the fluid - component interfaces only. In the inner portion of the ATS element the radiative rays are physically intercepted and multiply reflected by the component itself. However, a small contribution related to the immediate portion of the component near the boundaries could propagate outside. As a function of the ATS element shape and peculiar geometry, it is possible to take into account this additional radiative energy contribution through the corrective factor. Furthermore, as a consequence of the multiple reflections occurring inside the ATS component, the portions of the line upstream and downstream a typical porous domain can be considered independent and decoupled in terms of radiative effects. Most of the radiation rays are intercepted by the ATS component and can not propagate through it. In order to reproduce such behaviour within the simulation framework, the modeling methodology is further extended: a limiting function is formulated and can be applied. If the limit is active, the absorption coefficient of the fluid is artificially increased in the cells corresponding to the internal region of the porous domain, leading to a considerable decrease of the extinction coefficient Γ. This modification affects the resolution of the RTE: it allows to obtain a significant decrease of the incident radiation in correspondence of the inner porous region and to decouple the radiative heat transfer phenomena occurring in the porous domain upstream - downstream portions of the ATS line.

A proper boundary condition is implemented, so that the radiative energy content associated to the ATS component radiative emission is taken into account and its effect on the component temperature can be evaluated. In particular, according to equation (5), the corresponding heat

flux is imposed to the porous region boundaries. However, a consistent evaluation of the related incident radiation is required: the fluid G field is computed, than the values in correspondence of the porous domain boundaries are used for the heat flux computation. The obtained G values are affected by the introduction of the coupling source term, that must be subtracted to the boundaries G evaluation not to overestimate the corresponding incident radiation. The final expression of the estimated radiative heat flux is shown in equation (7).

$$q_w = \frac{\epsilon_w}{2(2-\epsilon_w)} \cdot (C_f \cdot 4e_b - (G_w - S_g)) \tag{7}$$

The described radiative coupling methodology is general and can be applied to all kind of ATS components modelled as porous media.

3. Case study

The CFD investigation is carried out on a simplified exhaust line. Such configuration is employed to perform a detailed thermal assessment and validation of the thermal transient of the EHC and of the simplified exhaust system, excluding all the additional complexity associated to the presence of the after-treatment components, as a TWC or particulate filters. The geometry consists of the primary exhaust manifolds, the EHC and the final portion of the line. The experimental test bench is instrumented with K-type thermocouples to measure the temperature of the flow inside the line, while two internal thermocouples are employed to determine the temperature of the EHC in correspondence of its central point and of its periphery. The axial coordinate at which the EHC measurement points are reffered to corresponds to half of the EHC length. A schematization of the considered geometry is presented in Figure 2, highlighting the position of the K-type thermocouples, referred to as T1, T2 and T3, and the location of the two EHC measurement points.

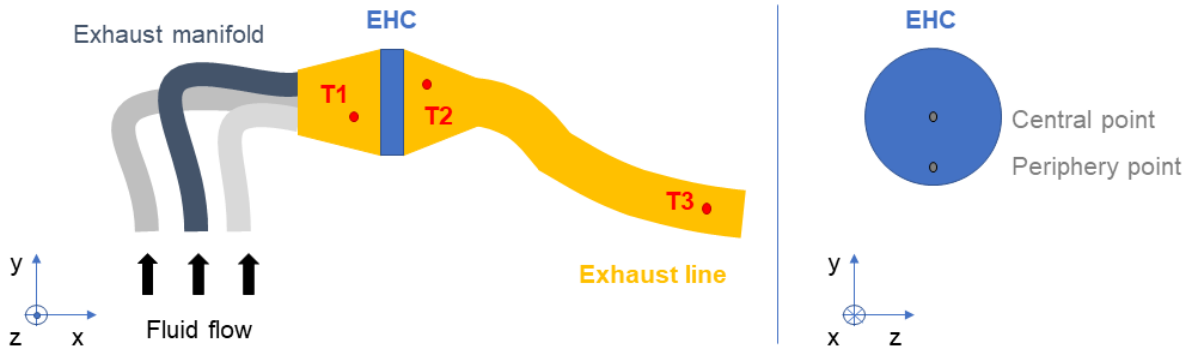

Figure 2: Case study geometry schematization

Three experimental tests are carried out on the considered geometry. The details of the different operating conditions are presented in table 1. Each experimental test is associated with a different electrical power and a different time range for which the power is supplied to the EHC. A generic test can be divided in three main phases:

- EHC on, no air flow inside the line
- EHC on, air flow inside the line
- EHC off, no air flow inside the line

According to the multi-region framework, the considered computational domains are related to the fluid, the EHC and the thermocouples regions. In particular, the addition of the measurement devices dedicated to characterize the fluid temperature provides a direct source of comparison between the experimental data and the simulated results [7].

Table 1: Experimental conditions, overview

Test	1	2	3
Electrical power [kW]	2.0	4.0	8.6
EHC on, zero flow [s]	102.0	17.0	9.5
EHC on, flow [s]	0.0	44.0	44.0
EHC off, zero flow [s]	90.0	26.5	34.0
Total test duration [s]	192.0	87.5	87.5
Air mass flow rate [kg/h]	0.0	45.0	45.0

The computational mesh is generated through snappyHexMesh, that is one of the automatic mesh generators provided by OpenFOAM. The fluid domain consists of $4.8 \cdot 10^6$ cells, while the EHC and thermocouples regions of $5.1 \cdot 10^5$ and $2.9 \cdot 10^4$ cells respectively. A visualization of the obtained computational domain is presented in Figure 3; in order to better appreciate the location of the components of interest, as the EHC and the K-thermocouples, the exhaust manifolds are excluded from the visualization. Two sections of the domains are presented, providing some details regarding the generated computational grid.

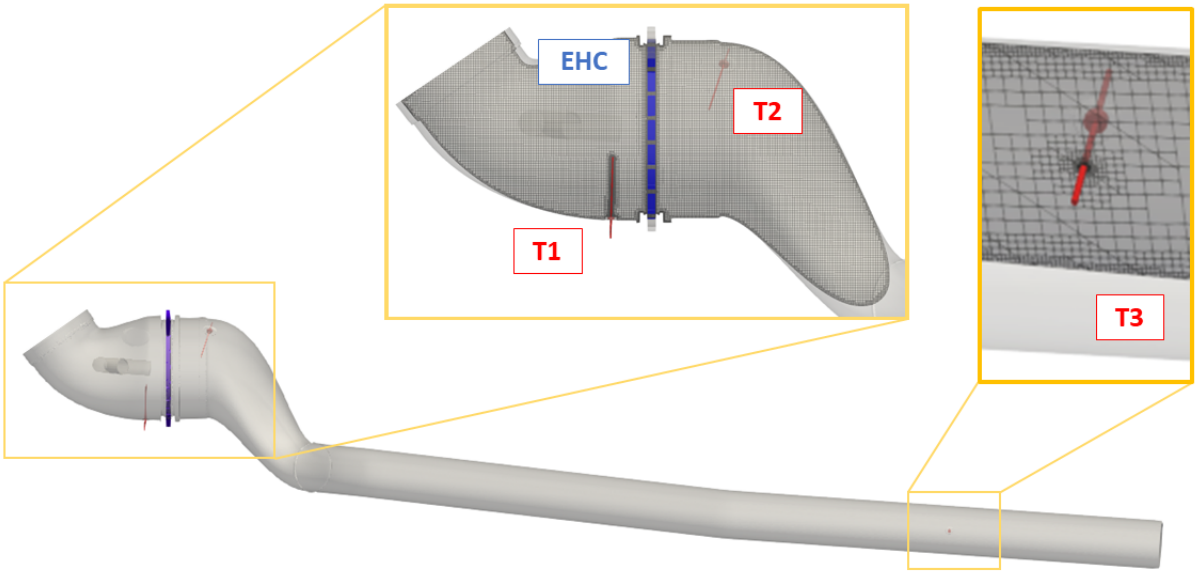

Figure 3: Case study computational domain

The time varying experimental conditions, in terms of fluid mass flow rate, fluid temperature and EHC voltage are imposed as boundary conditions. In this context, the implemented computational framework allows to directly compute the electrical power of the EHC, given the voltage boundary conditions and the material conductivity, by solving the differential formulation of the Joule heating effect. Regarding the thermal description of the walls, an OpenFOAM boundary condition is considered, taking into account the external convective heat transfer and the heat conduction through a given thickness of material characterized by a given thermal conductivity. The employed turbulence model is the standard $k-\omega$ SST with automatic wall treatment.

4. Results and discussion

The results of two different simulations are presented for each operating condition. At first, the standard CHT simulation methodology is applied; then, the simulation is replicated adopting the proposed radiation modeling. The comparison with the experimental data allows to appreciate the effects of the novel radiative coupling methodology. The results are presented in a non-dimensional form, analyzing each temperature profile through a temperature ratio, defined as follow:

$$T_{ratio,i} = \frac{T_i - T_{min}}{T_{max} - T_{min}} \tag{8}$$

where T_i is the temperature of the i thermocouple, T_{max} and T_{min} the chosen reference maximum and minimum temperatures.

The thermal validation of the system is carried out comparing both the temperature profiles of the three K-type thermocouples (T1, T2 and T3) and the profiles associated to the EHC internal points (center and periphery). Referring to the implemented radiation modeling described in Section 2.2 and to Equation (6), a corrective factor C_f equal to 1.25 is considered for all the experimental conditions. As example, the spatial distributions of the EHC voltage and electrical power are presented in Figure 4. Figure 5 shows a similar visualization of the fluid domain velocity and temperature distributions. The visualizations are proposed through a section of the overall computational domain after the first 20 seconds of the second experimental test.

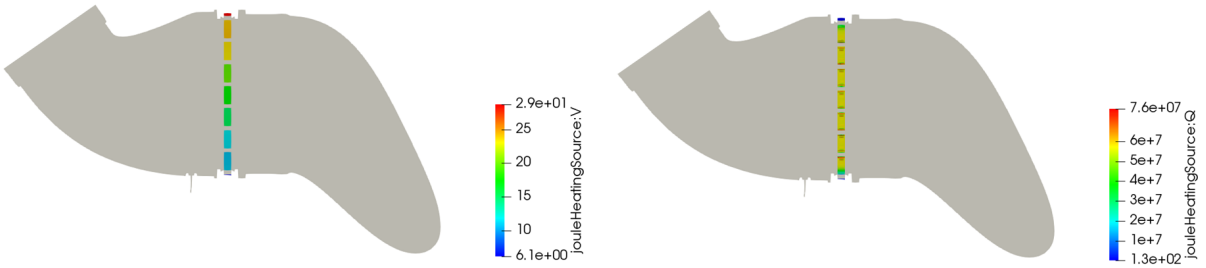

(a) *Voltage distribution* **(b)** *Electrical power distribution*

Figure 4: EHC fields visualization

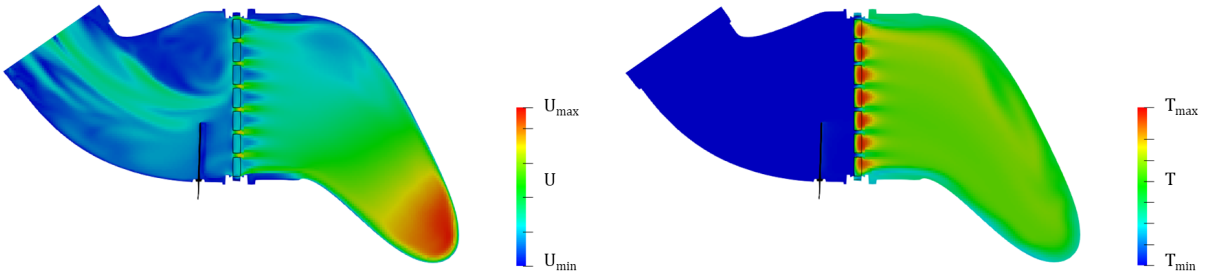

(a) *Velocity distribution* **(b)** *Temperature distribution*

Figure 5: Fluid fields visualization

4.1. Experimental test 1: 2.0 kW

The first experimental test is conducted in order to characterize the thermal transient of the line when no air flow is circulating. The extended time period for which the electrical energy is supplied to the component allows to highlight the importance of introducing a detailed radiation modeling for the porous domain. As shown in Figure 6, the description of the radiative heat transfer when no air flow is circulating inside the line is fundamental for a consistent simulation of the thermal transient of the EHC. The standard CHT methodology can represent the thermal interaction occurring between the air inside the line and the substrate through natural convection and conduction only. However, such contributions does not provide an accurate characterization of the temperatures of the EHC: the standard simulation shows a quasi-constant increase of both the EHC measurement points, leading to a significant overestimation of the temperatures. The maximum simulated temperature is about twice the maximum experimental value for both the EHC internal points. However, a maximum T_{ratio} equal to 1.2 is chosen for Figure 6, so that the comparison with the experimental data can be effectively appreciated.

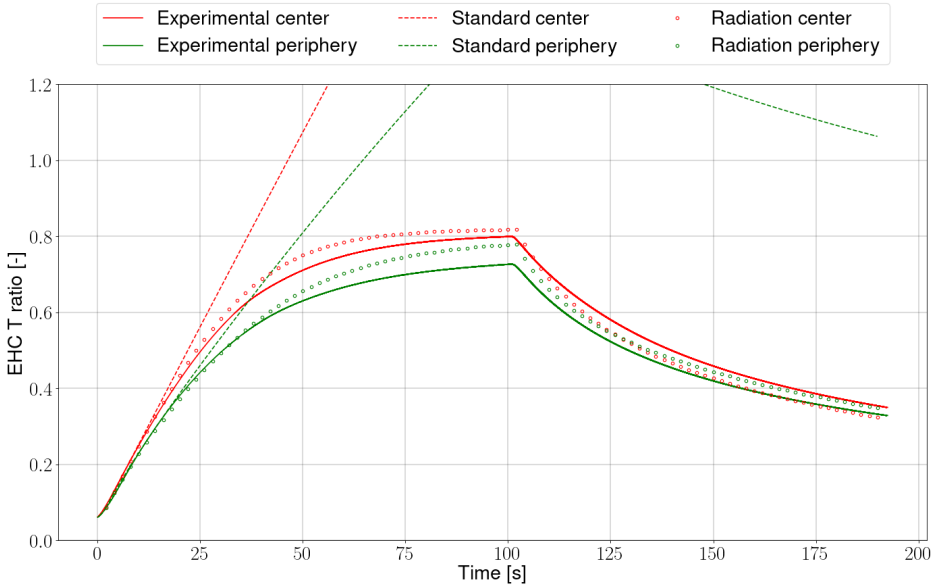

Figure 6: EHC Temperature profiles, 2 kW

The novel radiation coupling methodology allows to consistently reproduce the experimental EHC thermal transient. In this context, the description of the EHC radiative emission is fundamental for the simulation of the thermal transient of the component. The simulated maximum temperature of the central probe is consistent with the experimental value, while the peripherical point is affected by a slight overestimation.

Figure 7 presents the comparison related to the the K-type thermocouples. Both the standard and the radiation simulations are affected by an overestimation of the T1 and T2 temperature profiles. However, some improvements can be noted according to the radiation modeling. The temperature overestimation is significantly reduced for most of the considered time range.

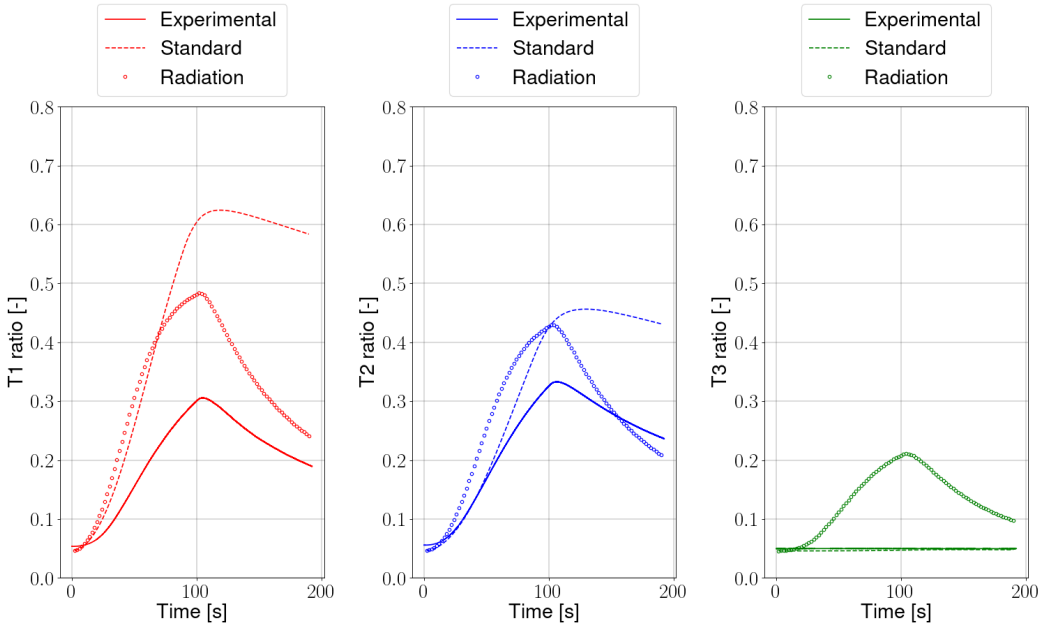

Figure 7: Thermocouples Temperature profiles, 2 kW

The T3 thermocouple simulated profile provides a direct proof of the P1 radiation model limitations. The simplified exhaust line geometry is such that the EHC emitted radiative rays can not interact with the T3 thermocouple; as a consequence, the experimental profile shows a time - constant temperature. However, the applied simulation methodology describes the radiation propagation through the incident radiation diffusion equation. According to such modeling, the EHC radiative emission propagates till the T3 thermocouple, that consequently shows a considerable temperature increase.
In case of a real EHC application in a typical ATS, the limit function described in section 2.2 could make up for the observed P1 limitation. In particular, the limit would be applied to the traditional substrate, located downstream the EHC, and it could effectively decouple the radiation propagation in the substrate upstream - downstream portions of the after-treatment line.

4.2. Experimental test 2: 4.0 kW

The second test is characterized by an intermediate level of electrical power. During the test second phase, the air flow rate interacts for a significant time interval with the component.
A coherent description of the EHC thermal transient is obtained for both the simulation methodologies, as presented in Figure 8. The EHC test second phase (17.0 - 44.0 seconds) is featured by an overall cooling, as a consequence of the thermal interaction between the cold air flow and the hot component. However, the proposed radiation modeling allows to reduce the overestimation affecting the standard simulation and to obtain a better match with the experimental data. The EHC temperatures are such that the radiative heat transfer contribution is significant for the component thermal transient. Such improvements can be noted analyzing the temperature peak at the end of the first test phase and the overall temperature trend of the second phase.

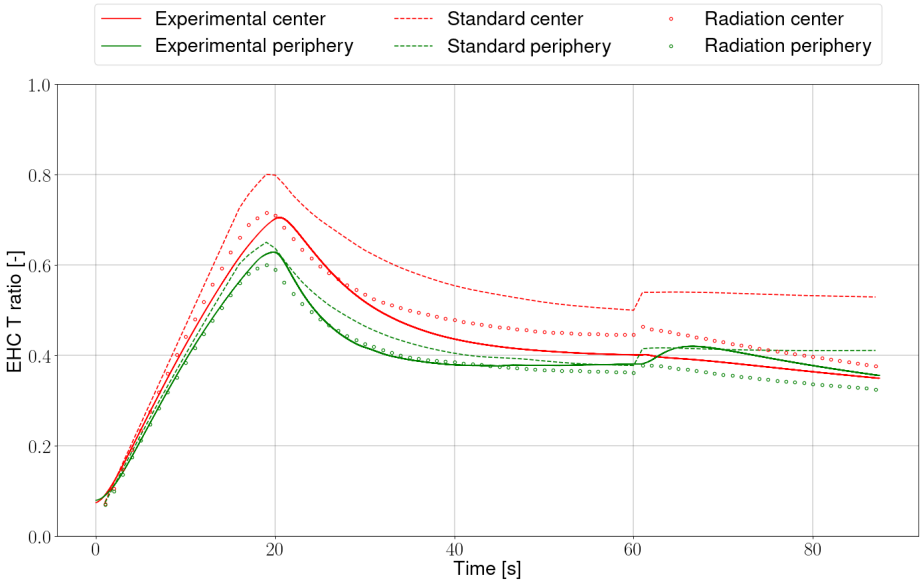

Figure 8: EHC Temperature profiles, 4 kW

As for the EHC thermal transient, the description of the radiative heat exchange phenomena allows to improve the K-type thermocouple results obtained by means of the computational framework. Figure 9 shows the T1, T2 and T3 temperature profiles. As previously described, the EHC thermal transient obtained through the standard simulation is affected by an overestimation with respect to the experimental data. Such overestimation is responsible for the higher temperatures of the T2 and T3 thermocouples: their thermal evolution is strictly dependent on the air flow convective heat transfer, while the air temperature is significantly affected by the EHC temperature field. For this reason, the improved description of the EHC temperatures results in an improved characterization of the T2 and T3 thermal transient. The radiation modeling leads also to improvements on the T1 temperature profile.

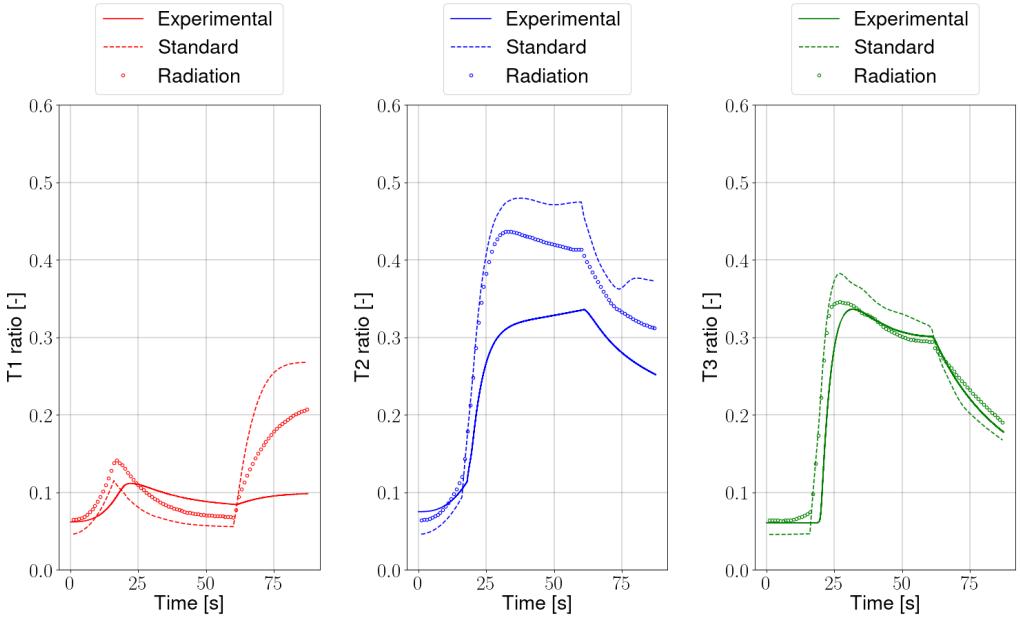

Figure 9: Thermocouples Temperature profiles, 4 kW

4.3. Experimental test 3: 8.6 kW

The third experimental test is composed of a short first phase, where 8.6 kW are supplied to the EHC at zero flow condition. In the second phase the air flow rate interacts with the EHC for a significant amount of time. Similarly to what can be observed for the results of the 4.0 kW experimental conditions, the outcome of the test second phase (9.5 - 44.0 seconds) is an overall cooling of the EHC. As presented in Figure 10, the standard simulation is not able to represent such thermal behaviour: the temperature of the central probe increases for the whole duration of the considered test phase, causing a significant overestimation of the EHC temperature values. Instead the implemented radiation modeling allows to correctly describe the thermal transient of the component, providing a good match with the experimental data.

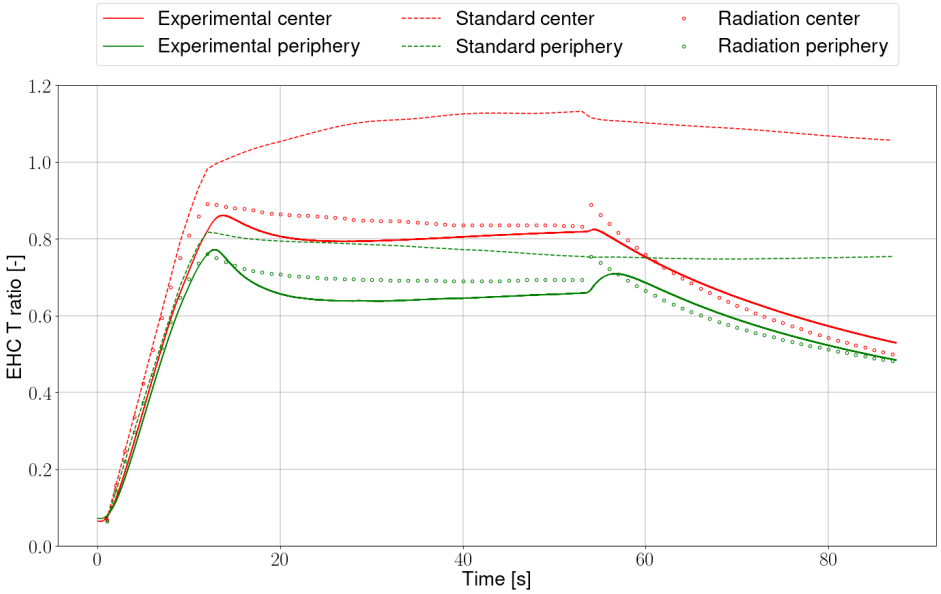

Figure 10: EHC Temperature profiles, 8.6 kW

During the first phase of the test, the simulated profiles of the T1, T2 and T3 thermocouples show similar trends for both the standard and the radiation simulations. However, once the air flow rate is activated, some differences can be noted, as depicted in Figure 11.

In particular, during the test second phase, the experimental profile of the T1 thermocouple is characterized by a slow increase of its temperature. The observed behaviour is the outcome of the superimposition of two different phenomena: the thermocouple cooling, due to its interaction with the cold air flow, and its heating, due to the propagation of the EHC radiative rays and the consequent radiative heat transfer. As previously stated, the standard simulation methodology describes the thermal transient of the considered component through convection and conduction only. As a consequence, a rapid decrease of the device temperature is obtained (9.5 - 25.0 seconds). The implemented radiation modeling, and in particular the addition of the incident radiation source term in the fluid RTE, provides the description of the EHC radiative rays propagation to the T1 thermocouple, resulting in a more coherent representation of its thermal transient.

The T2 and T3 temperature profiles are strictly dependent on the convective heat transfer caused by the air flow and the measurement devices interaction. The standard simulation methodology provides an overestimation of the EHC temperature field; the resulting higher air flow temperatures are responsible for the observed T2 and T3 thermocouples thermal behaviour. This effect can be noted analyzing both the slope of the thermocouples temperature profile and their absolute values. As previously described, the radiative coupling methodology

provides a more accurate description of the EHC temperature field. According to the radiation simulation, as a consequence, the T2 and T3 temperature profiles are in good agreement with the experimental data.

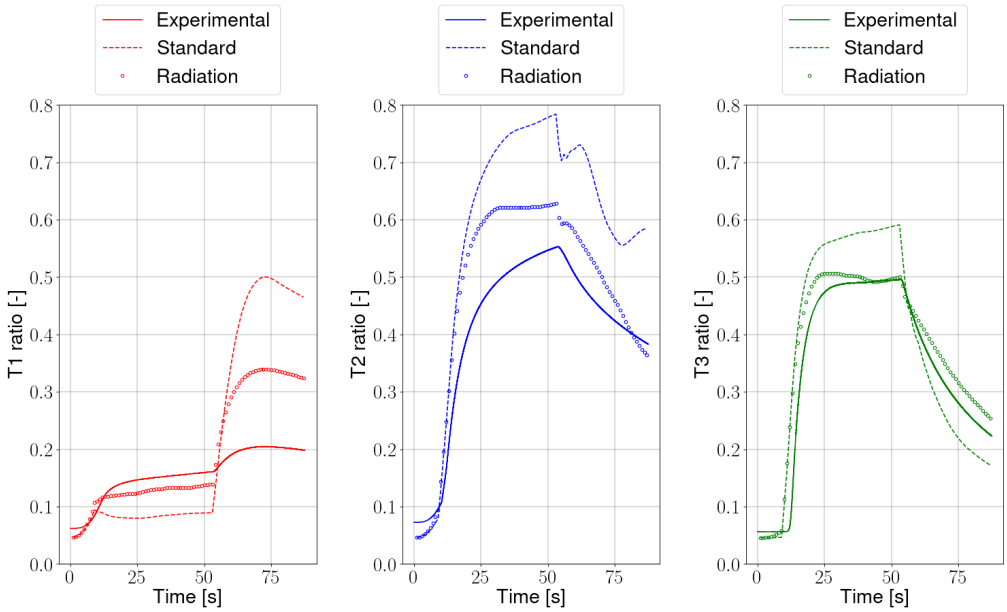

Figure 11: Thermocouples Temperature profiles, 8.6 kW

5. Conclusions

A CFD CHT multi-region modeling approach has been extended so that the computational methodology can account for the radiative heat transfer phenomena taking place in correspondence of porous ATS components.

The implemented model allows to describe the component emitted radiative rays propagation, so that their interaction with the solid regions of the computational domain can be taken into account. In addition, an accurate description of the radiative heat flux at the fluid - ATS element interface is provided, as well as its effect on the component temperature field.

The proposed radiative coupling methodology has been applied for the estimation of the thermal transient of a simplified ATS, equipped with an EHC, for three different operating conditions. As a result, the radiative coupled simulations provided a rather satisfactory match with the available experimental data. The comparison between the standard and the extended methodology allows to appreciate how the description of the radiative heat transfer phenomena was required for an accurate characterization of the exhaust line thermal behaviour.

However, the employed base radiation model (P1) is intrinsically associated to some limitations. As a further development, the implemented radiative coupling procedure could be extended with the adoption of more complex radiation models, such as the finite volume discrete ordinate methods (fvDOM).

References

[1] Mahadevan G and Subramanian G 2017 *SAE Technical Paper* 2017-01-2367
[2] Joshi A 2021 *SAE Technical Paper* 2021-01-0575
[3] Raffael H, Philipp E and Christopher O 2017 *Energies* **10** 1548
[4] Eisazadeh-Far K and Younkins M 2022 *SAE Technical Paper* 2016-01-0672
[5] Hassdenteufel A, Schünemann E, Neubert V and Hirchenhein A 2022 *J. Transp. Eng.* **8** 100-109
[6] Della Torre A, Barillari L, Montenegro G, Onorati A, Rulli F, Paltrinieri S, Rossi V and Pulvirenti F 2021 *SAE Technical Paper* 2021-24-0089
[7] McCarthy J Jr, Matheaus A, Zavala B, Sharp C and Harris T 2022 *SAE Technical Paper* 2022-01-0539
[8] Velmurugan D, McKelvey T O and Olsson J 2022 *SAE Technical Paper* 2022-01-0544
[9] Brück R, Lienou L I, Schatz A and Ellmer D 2020 *29th Aachen Colloquium Sustainable Mobility*
[10] Bargman B, Jang S, Kramer J, Soliman I, Abubeckar M S and Abhid A 2021 *SAE Technical Paper* 2021-01-0572
[11] Della Torre A, Montenegro G, Onorati A and Cerri T 2018 *SAE Technical Paper* 2018-01-0961
[12] Della Torre A, Montenegro G, Onorati A, Cerri T, Tronconi E and Nova I 2020 *SAE Technical Paper* 2020-01-0356
[13] Sazhin S S, Sazhina E M, Faltsi-Saravelou O and Wild P 1996 *Fuel* **75** 289-294
[14] Crnjac P, Škerget L, Ravnik J and Hribersek M 2017 *Int. J. of Comput. Methods Exp. Meas.* **5** 348-358
[15] Raithby G D and Chui E H 1990 *J. Heat Transfer* **112** 415-423
[16] Siegel R and Howell J R 1992 *Thermal Radiation Heat Transfer* (Washington DC: Hemisphere Publishing Corporation)